# Large-Scale Preconditioning of Deep-Water Formation in the Northwestern Mediterranean Sea

GURVAN MADEC,* FRANÇOIS LOTT,+ PASCALE DELECLUSE,* AND MICHEL CRÉPON*

*Laboratoire d'Océanographie Dynamique et de Climatologie, Unité mixte de recherche CNRS/ORSTOM/UPMC, Université Paris VI, Paris, France

+Laboratoire de Météorologie Dynamique, CNRS, Paris, France

(Manuscript received 12 September 1994, in final form 25 July 1995)

ABSTRACT

The large-scale processes preconditioning the winter deep-water formation in the northwestern Mediterranean Sea are investigated with a primitive equation numerical model where convection is parameterized by a nonpenetrative convective adjustment algorithm. The ocean is forced by momentum and buoyancy fluxes that have the gross features of mean winter forcing found in the MEDOC area. The wind-driven barotropic circulation appears to be a major ingredient of the preconditioning phase of deep-water formation. After three months, the ocean response is dominated by a strong barotropic cyclonic vortex located under the forcing area, which fits the Sverdrup balance away from the northern coast. In the vortex center, the whole water column remains trapped under the forcing area all winter. This trapping enables the thermohaline forcing to drive deep-water formation efficiently. Sensitivity studies show that $\beta$ effect and bottom topography play a paramount role and confirm that deep convection occurs only in areas that combine a strong surface thermohaline forcing and a weak barotropic advection so that water masses are submitted to the negative buoyancy fluxes for a much longer time. In particular, the impact of the Rhône Deep Sea Fan on the barotropic circulation dominates the $\beta$ effect: the barotropic flow is constrained to follow the bathymetric contours and the cyclonic vortex is shifted southward so that the fluid above the fan remains quiescent. Hence, buoyancy fluxes trigger deep convection above the fan in agreement with observations. The selection of the area of deep-water formation through the deflection of the barotropic circulation by the topography seems a more efficient mechanism than those associated with the wind-driven barotropic vortex. This is due to its permanency, while the latter may be too sensitive to time and space variations of the forcing.

## 1. Introduction

The northwestern Mediterranean Sea is one of the few midlatitude ocean basins where deep water forms in winter. This formation is primary triggered by atmospheric conditions. During winter, strong, cold, and dry continental winds blow from the north and the northwest down the Rhône Valley (the mistral) and the sill separating the Pyrénées from the Massif Central mountains (the Tramontane). They are responsible for high evaporation and strong cooling that increase the surface density and drive deep convection (MEDOC Group 1970). Several other factors have been invoked in order to explain the selection of this specific area for deep-water formation (DWF). The first one is the local ocean circulation and density structure. The northwestern Mediterranean Sea is characterized throughout the year by a regional cyclonic circulation (Gascard 1978; Crépon et al. 1982). In the center of that large gyre a cyclonic vortex of about 100 km in diameter appears every winter (Anati and Stommel 1970; Swallow and Gaston 1973). This vortex defines the specific area for DWF (Gascard 1978) since both the weakness of the horizontal advection in the vortex center and the associated dome of isopycnal surfaces contribute to enhance deep convection in response to atmospheric forcing. The second factor is the existence of a source of salt in subsurface, the Levantine Intermediate Water (Gascard 1978). As the depth of convection reaches this water mass, the salinity and temperature of the upper ocean mixed layer increase. This in turn allows the density to become higher and induces a local increase of thermohaline fluxes as the air–sea temperature difference becomes larger. The third factor is the presence of small cyclonic eddies of diameter of some kilometers (chimneys) linked to meander development at the edge of the front that defines the vortex (Killworth 1976). Gascard (1978) suggests that the weak reserve of buoyancy of these chimneys creates very favorable conditions for deep convection in their centers. The last factor is the topography effect. Swallow and Gaston (1973) first suggested that the Rhône Deep Sea Fan

*Corresponding author address:* Dr. Michel Crépon, CNRS/ORSTOM/UPMC, LODYC, Universite Pierre and Marie Curie, 4 Place Jussieu, Paris, Cedex 75252 France.



© 1996 American Meteorological Society

might trap and enhance the preconditioning phase vortex (Fig. 1). Hogg's (1973) theoretical study supported this conclusion. He analyzed the problem within the framework of the formation of a baroclinic Taylor column for weakly stratified fluid. When a narrow baroclinic coastal current, flowing westward at the surface and eastward near the bottom, passes a conical bump abutted to the continental slope, the topography induces the formation of a surface cyclonic vortex trapped over the bump when the stratification is weak. The trapping of central vortex water and the dome of isopycnal surfaces associated with the vortex combine to enhance the deep convection (and thus DWF) driven by the cooling of the surface water.

In a numerical study of the DWF in the northwestern Mediterranean Sea, Madec et al. (1991a) have suggested that the local thermohaline forcing is sufficient to destroy the ocean stratification and drive deep convection. The cyclonic vortex surrounding the deep convective area appears, in their study, as a result of the DWF, not as a prerequired condition. The shape and location of the vortex are entirely determined by the spatial characteristic of the thermohaline forcing they consider. They also found that the vortex are baroclinically unstable. Meanders, 40 km in wavelength, develop around the vortex in agreement with the observations (Gascard 1978; Crépon et al. 1982). They contribute to deep-water formation by amplifying vertical motions, but tend to restabilize the surface water by horizontal advective motions. Moreover, in a high-resolution sensitivity study Madec et al. (1991b) have shown that strong thermohaline forcing events tend to stop meander development while they enhance local convective processes as described by Jones and Marshall (1993). The baroclinic instability thus appears to be a process of spreading of newly formed deep water rather than a preconditioning mechanism. In a third study dealing with a more realistic thermohaline forcing shape, which simulates the mistral pattern (the maximum of the forcing being at the coast), Madec and Crépon (1991) found that the vortex can result from interaction between the buoyancy-driven circulation and Kelvin wave dynamics along the northern coast.

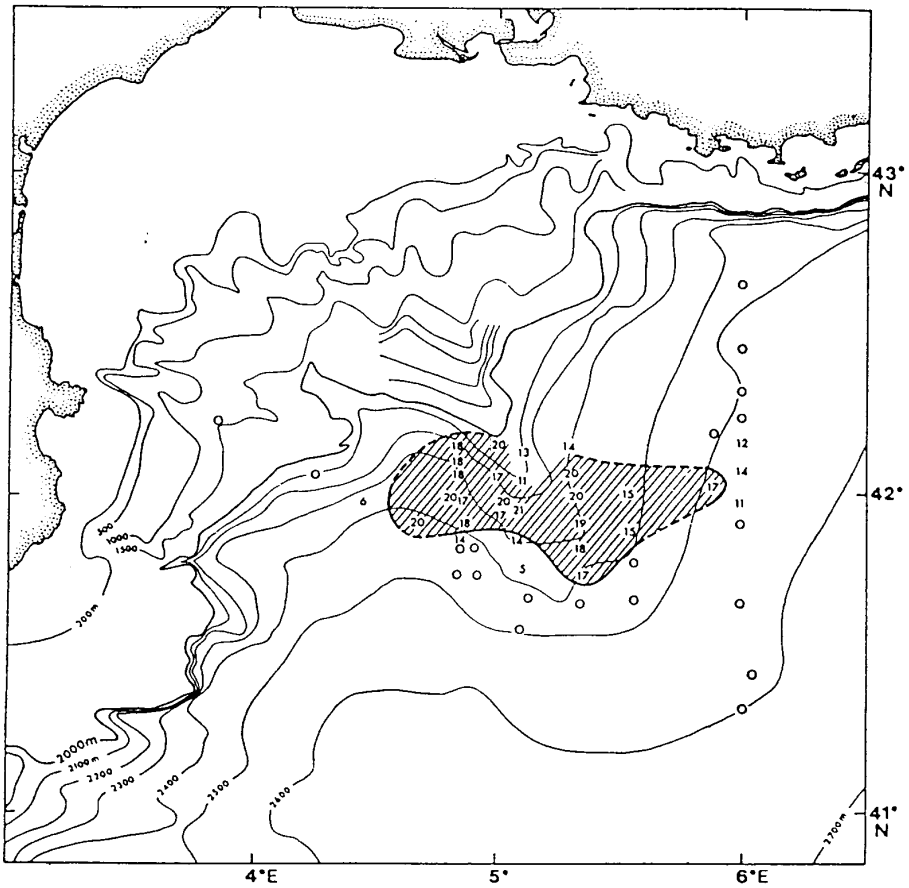


FIG. 1. Depth of the mixed layer (potential temperature constant within ±0.02°C) in hundred of meters. From observations during 16–21 February 1969. Open circle indicates absence of deep mixing. From Swallow and Caston (1973).

All these studies show that the thermohaline forcing is a major component of the local winter dynamics of the northwestern Mediterranean Sea. Nevertheless, such a forcing is related to evaporation via a loss of latent heat and water vapor, which depends on the strength of the wind. As strong thermohaline forcing is always associated with strong wind stress, it can be thought that the wind-driven circulation has some impact on the DWF process. This effect could be important since the ocean response to the wind is rapid and has a strong barotropic component, while the response to the thermohaline forcing is slow and mainly baroclinic (Crépon et al. 1989). The existence of a rather strong (6 cm $s^{-1}$) barotropic component in the ocean circulation of the MEDOC area has recently been found on current meter records (Schott and Leaman 1991). Moreover, the observed barotropic circulation seems to roughly follow the bathymetric contours suggesting an influence of the bottom topography on the DWF process.

In the present paper we try to tie the different pieces of the puzzle together in order to get a synthetic view of the different large-scale processes affecting the preconditioning phase of DWF. The small-scale processes associated with deep convection have recently been reanalyzed (Jones and Marshall 1993; Send and Marshall 1993) and are beyond the scope of this paper. The convection is simply parameterized by a nonpenetrative convective algorithm that is consistent with winter observations in the MEDOC area (Anati 1971). This parameterization has proved successful in previous studies (Madec et al. 1991a, 1991b) and appears to give mesoscale results that are in good agreement with more sophisticated parameterization schemes (Schott et al. 1993). After a presentation of the numerical model in section 2, the effect of wind stress versus thermohaline forcing is studied in section 3 in a flat rectangular basin. A sensitivity study to the $\beta$ effect and topography is studied in section 4. The overall significance of the numerical results is discussed in the last section.

## 2. Model description

This study is performed with the finite difference primitive equation OPA model developed at LODYC (Andrich et al. 1988; Madec et al. 1991a; Delecluse et al. 1993). It is a finite difference C-grid three-dimensional model written in a tensorial formalism (Marti et al. 1992). A detailed description of the model equations can be found in Delecluse et al. (1993). Let us just discuss the parameters and model physics specific to the numerical experiments presented in this paper. The vertical coordinate can be either a $z$ coordinate, or a stretched (terrain following) coordinate, or a hybrid $z$-stretched coordinate (Lott et al. 1990). The implementation of two latter coordinates is similar to that as Gerdes (1993). They are introduced in order to avoid uncomfortable problems with the lower boundary condition in the presence of bottom topography. The truncation error that appears in the horizontal pressure gradient is minimized by splitting the pressure into its initial value and its departure from this value (Gary 1973). The initial pressure gradient is then computed in $z$ coordinate, while for the departures, this gradient is computed in the stretched or hybrid coordinate. A similar procedure is used for the horizontal diffusion of heat and salt.

The density field is computed from temperature and salinity fields by a nonlinear state equation (Eckart 1958). Subgrid-scale physics is parameterized by a second-order operator. The horizontal eddy viscosity and diffusivity coefficients are equal to 80 $m^2\ s^{-1}$, while the vertical ones are assumed to vary as a function of the local Richardson number, according to the parameterization proposed by Pacanowski and Philander (1981). They range from molecular viscosity to a maximum value of $10^2$ $cm^2\ s^{-1}$ when the Richardson number is zero.

Convective processes are parameterized by a nonpenetrative convective adjustment algorithm that instantaneously restores the static stability of the water column. The algorithm used mixes downward the statically unstable portion of the water column, but only until the density structure becomes neutrally stable (i.e., until the mixed portion of the water column has a density smaller or equal to the density of the water just below). A more detailed description can be found in Madec et al. (1991a). The algorithm ensures that static stability of the water column is reached at each time step. This property is of paramount importance since it avoids the existence of persisting unrealistic static instabilities at the sea surface (Killworth 1989). Note that momentum is not mixed through the convective adjustment algorithm but through the vertical diffusion of momentum since the Richardson-dependent formulation causes the vertical eddy viscosity coefficient to be maximum after a static adjustment.

For all the numerical experiments performed in this study, the ocean starts from rest with a horizontally homogeneous density field computed from temperature and salinity profiles typical of the offshore northwestern Mediterranean Sea conditions in early winter (Fig. 2). A cold and relatively fresh surface water overlies a warm and salty water between 200 and 600 m (the Levantine Intermediate Water) and a thick and weakly stratified layer of deep water. The model has 20 vertical levels whose separation varies from 10 m to 25 m in the upper 200 m, and reaches 400 m near the ocean bottom. The horizontal grid spacing is $1/24$ deg in latitude and $1/18$ deg in longitude (i.e., $\sim$4.5 km), which is smaller than the first baroclinic radius of deformation of the initial state (6.53 km).

In experiments I to IV, the model domain consists in a closed, flat rectangular ocean basin of 750 km $\times$ 400 km $\times$ 2.4 km centered at 42°N, which accounts for the MEDOC area. In experiment V, it is basically

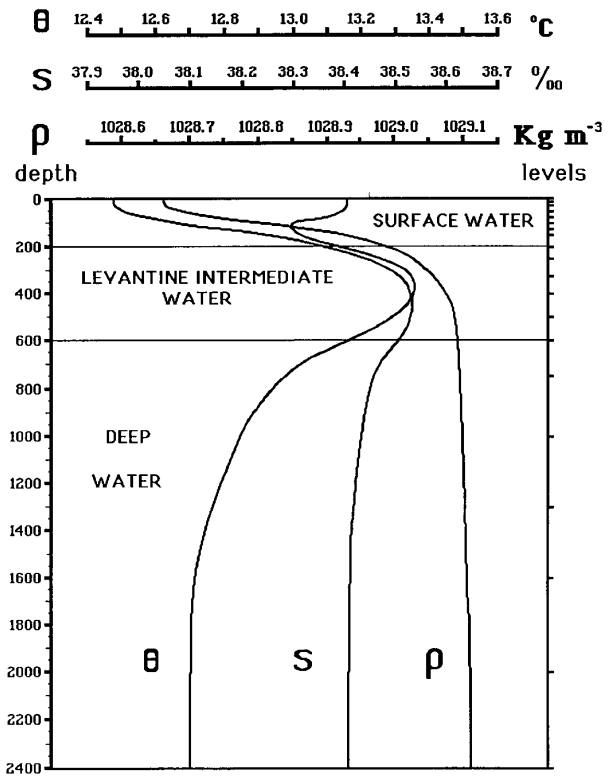


FIG. 2. Initial vertical structure for potential temperature, salinity, and potential density ($\sigma_\theta$ units) versus depth (on the left). The depth of the model vertical levels are indicated on the right of the frame.

the same ocean basin except that two bathymetric features have been added. First, the northern coastline is shifted 100 km southward, while a trapezoidal continental shelf of constant depth (100 m) simulates the Golfe du Lion (Fig. 3) at the northern part of the basin. The shelf is connected to the deep ocean through a continental slope of 40-km meridional extension across which the ocean depth varies from 100 m at $y = 340$ km to 800 m at $y = 300$ km. Second, in the deep ocean, a deep conic bottom topography is introduced, abutted to the continental slope (Fig. 3). This topography accounts for the Rhône Deep Sea Fan. It is defined by the following bottom elevation:

$$h(x, y) = \begin{cases} H_0 \cos^2\left(\dfrac{\pi R}{2R_0}\right) & \text{for} \quad R^2 = (x - x_0)^2 \\ & \qquad + (y - y_0)^2 < R_0^2 \\ 0 \quad \text{elsewhere,} \end{cases}$$

where $H_0 = 1000$ m is the height of the fan, $R_0 = 100$ km is its horizontal extension, and $(x_0, y_0) = (425$ km, 300 km) is the location of its top.

A $z$ coordinate is used for the flat bottom ocean, while a hybrid vertical coordinate is used when dealing with a variable bottom topography. The hybrid coordinate consists of a stretched coordinate between the ocean bottom and 400 m and of a $z$ coordinate above. In that configuration, the stretched coordinate is only introduced under the main pycnocline, in a weakly stratified zone. This strongly contributes to reduce the truncation error associated with the pressure gradient. In particular, on the shelf, the model has five horizontally uniform vertical levels and a $z$ coordinate is used to fit the steep continental slope in order to avoid numerical problems that can arise with sharp variations in stretched coordinate (Gary 1973).

The five numerical experiments were performed over a four-month winter period. They differ either by the forcing fields, the Coriolis parameter, or the basin geometry used (Table 1). The ocean was first forced by a wind stress field only (experiment I), then by evaporation and heat flux fields (experiment II) and by all of these forcing fields in experiments III, IV, and V. These forcings are applied over a tongue-shaped area (200 km $\times$ 300 km) (Fig. 4a), which approximately fits the shape of the mistral and Tramontane (Meteorological Office 1962). After a 60-h rise period, they are assumed to be constant until the end of the fourth month. The thermohaline flux consists of an ocean heat loss of 170 W m$^{-2}$ and a salt flux corresponding to a loss of fresh water of 6.3 mm d$^{-1}$. The wind is formed by a northern wind stress field of 0.17 Pa in magnitude. These are the mean winter values deduced from the monthly mean estimations given by Bunker (1972) and May (1982) for the MEDOC area. In Experiment IV, the $\beta$ effect is suppressed, while experiment V uses a different basin geometry. Note that in the latter experiment, an input of freshwater (negative salt flux) has been added over the continental shelf (i.e., north of $y = 340$ km) in order to parameterize the river runoff (Fig. 4b). The surface-averaged salt flux over the continental shelf corresponds to the mean winter balance

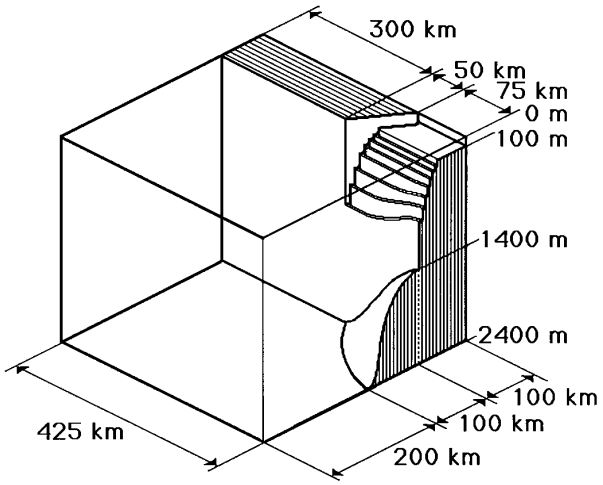


FIG. 3. Half ocean basin geometry used in experiment V.

between an evaporation of 6.3 mm $d^{-1}$ and a river runoff of 2100 $m^3 s^{-1}$, which represents the mean Rhône River discharge (Fieux 1972).

## 3. Wind versus thermohaline forcing response

The ocean responses to the wind stress forcing and to the thermohaline forcing are very different. The latter forcing directly acts on the $T-S$ characteristics of the seawater, and thus on the density field. This in turn modifies the pressure field and generates a baroclinic ocean response (Crépon et al. 1989). In spite of the strong heat flux and evaporation occurring in winter in the Mediterranean Sea, this process evolves slowly due to the large heat capacity of seawater. In contrast, the wind acts directly and rapidly on the velocity field through momentum fluxes at the sea surface and Ekman pumping effect, but it cannot generate deep mixing as thermohaline fluxes do. The mass redistribution associated with the wind-driven advection can be of importance and in turn influences the convection. To deepen our understanding of these actions let us investigate the ocean response to these different forcings through a set of sensitivity experiments.

### *a. Response of the ocean to the wind stress forcing (experiment I)*

The wind stress field considered here has two cells of negative and positive curl located at the western and eastern sides of the forcing area acting as two sources of negative and positive vorticity for the ocean. The barotropic and the baroclinic ocean responses are very different due to the large time difference for adjustment, which is linked to the large difference between barotropic and baroclinic Rossby wave speeds.

Let us first examine the barotropic response of the ocean. The ocean reacts rapidly to the application of the vorticity sources. After a short transient period of some days, two barotropic gyres are generated. They slowly evolve toward a steady solution formed of a large cyclonic gyre located under the forcing area. This evolution is clearly observed on the barotropic streamfunction associated with the vertically averaged velocity (Fig. 5a). Let us consider an adjustment timescale $T_j = 1/\beta L$ for barotropic motion, which represents the time for a dispersive barotropic Rossby wave to travel

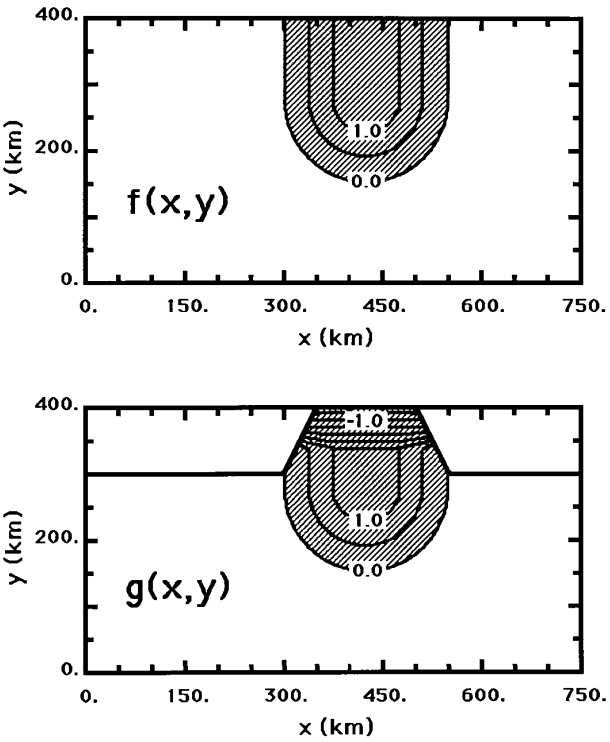


FIG. 4. Space forcing functions $f(x, y)$ and $g(x, y)$. For experiments II to V, the total heat flux $Q$ and the evaporation $E$ are given by $Q = Q_0 f(x, y)$ and $E = E_0 f(x, y)$, where $Q_0 = -170$ W $m^{-2}$ and $E_0 = -6.3$ mm $d^{-1}$ except in experiment V where the evaporation is given by $E = E_0 g(x, y)$. For all the wind-driven experiments the wind stress field is given by $\tau_x = \tau_0 f(x, y)$ and $\tau_y = 0$, where $\tau_0 = 0.17$ Pa.

a distance $L$. At small time ($t_s < 1/\beta L = 5 \times 10^5$ s = 6 days, where $L$ is a characteristic length scale of the forcing), the transient response is first dominant and the potential vorticity equation for the forced barotropic flow,

$$(\partial_t + u\partial_x + v\partial_y)\zeta + \beta v = \text{curl}(\tau)/\rho_0$$

reduces to

$$\partial_t \zeta = \text{curl}(\tau)/\rho_0.$$

Neglect of the nonlinear terms is justified by the weakness of the circulation at the beginning of the forcing period. Therefore, two barotropic gyres, a cyclonic one

TABLE 1. Characteristics of the five numerical experiments.

| Experiment | Wind stress | Thermohaline fluxes | $\beta$ effect | Continental shelf and Rhône Deep Sea Fan |
|---|---|---|---|---|
| I | yes | no | yes | no |
| II | no | yes | yes | no |
| III | yes | yes | yes | no |
| IV | yes | yes | $f$ = cste | no |
| V | yes | yes | yes | yes |

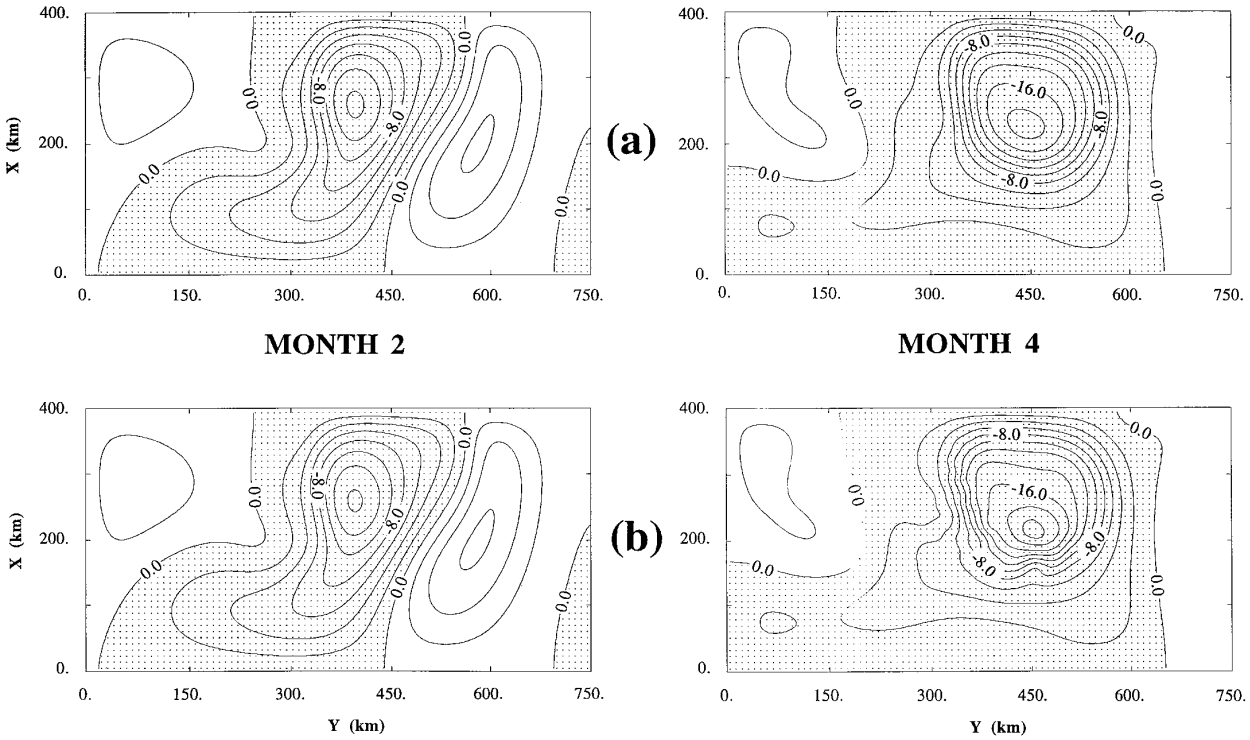


FIG. 5. Barotropic streamfunction at months 2 and 4 for (a) experiment I and (b) experiment III. Contour interval equals 2 Sv. The remarkably identical pattern between (a) and (b) shows that the wind is mainly responsible for the barotropic response, and that there is a weak interaction between the barotropic response and the baroclinic one.

and an anticyclonic one, are forced on the eastern and western sides of the forcing area under the zone of positive and negative vorticity sources. As time progresses, this solution evolves toward a steady circulation when the fast barotropic planetary Rossby waves have been radiated away. The anticyclone disperses westward while the cyclone shifts under the forcing area and reaches a steady state at $t_L \gg 1/\beta L$, which nearly fits the Sverdrup balance, $\beta v = \text{curl}(\tau)/\rho_0$, away from the northern coast. The input of positive (negative) vorticity under the area of positive (negative) wind stress curl generates a northward (southward) advection of planetary vorticity. The expected transport of the meridional currents resulting from the Sverdrup balance is

$$\Psi_{\max} = \tau_{\max}/(\rho_0\beta) = 17 \text{ Sv} \quad (1 \text{ Sv} \equiv 10^6 \text{ m}^3 \text{ s}^{-1}),$$

while the magnitude found after four months is one Sverdrup larger (Fig. 5a). This difference can be related to the accumulation of cyclonic vorticity in the cyclonic gyre during the transient period, which can modify the vorticity balance through the nonlinear advection of relative vorticity.

In the vicinity of the northern coast, the Sverdrup balance is not valid anymore since the meridional advection of planetary vorticity is stopped by the coastal boundary condition $v = 0$. The current leaves the area where the wind forcing is a source of positive vorticity and flows westward along the northern coast, following the cyclonic circulation initiated during the transient period. The width and intensity of the coastal current remain close to those found offshore below the positive vorticity source. Indeed, along the northern coast, the relative vorticity of the flow now becomes $\zeta \approx -\partial_y u$. It is of the same order of magnitude as the relative vorticity, $1/\beta\partial_x[\text{curl}(\tau)/\rho_0]$, acquired below the wind stress curl areas. This flow is able to conserve its relative vorticity (i.e., its width and intensity) since the planetary vorticity of a zonal flow is constant. A small exchange of vorticity occurs at the coast due to the no-slip boundary condition, but it is not an essential ingredient of the coastal dynamics, contrary to what happens along meridional coasts. As it penetrates the area of negative wind stress curl, the flow turns left and goes to the south to compensate the input of negative vorticity by the southward advection of planetary vorticity. In the south of the forcing area, the current flows eastward and closes the cyclonic circulation. Its intensity and width remain close to those acquired below the wind curl areas mainly by conservation of the relative vorticity acquired in these regions.

The resulting barotropic circulation pattern found after four months is thus formed of a single large cyclonic gyre located below the forcing area. Its transport is ~18

Sv (Fig. 5a) and the associated velocity is of several centimeters per second (Fig. 6a), reaching 8 cm $s^{-1}$ at month 4 (not shown).

Let us now examine the baroclinic response to the wind. The wind stress curl provides an upward Ekman pumping on the eastern side of the forcing area and downward on the western side inducing a pycnocline displacement of some ±50 m. During the first month it results in a pycnocline displacement presenting two broad antisymmetric structures, a bump in the east and a trough in the west (Fig. 7a). These structures are associated with two baroclinic eddies respectively, a surface cyclone associated with the bump and a surface anticyclone associated to the trough as found by McCreary et al. (1989). As these structures are embedded in a cyclonic barotropic field, they are slowly advected cyclonically around the forcing area (Fig. 7a) and their evolution is consequently different from that of the McCreary et al. study. The bump is progressively stretched northwestward and, after four months, occupies the whole coastal area below the forcing area and combines with the barotropic cyclone to reinforce the surface cyclonic circulation. The trough is stretched southeastward and progressively occupies the southern edge of the forcing area. A significant part of it is advected by the barotropic field outside this area, in the southwest (Fig. 7a).

### b. *Ocean response to the thermohaline forcing (experiment II)*

The response to the thermohaline forcing has been studied in detail in Madec and Crépon (1991) and is briefly discussed here. When only the thermohaline forcing is applied, surface waters within the forcing area slowly become colder, saltier, and thus denser than the surrounding waters. Vertical mixing occurs in the surface layers restoring the static stability of the water column and inducing a slow increase of the surface mixed layer. A patch of dense surface water is progressively formed whose horizontal pattern is linked to the forcing geometry (Fig. 7b). Interaction between the coast and the ocean circulation associated with spatial variation of the thermohaline forcing drives the detachment from the coast of the deep convective area (Madec and Crépon 1991). It is found from a linear analysis done with a two layer fluid that in the vicinity of the coast (i.e., at a distance of the order of the first internal radius of deformation) this detachment is linked to the generation of two baroclinic coastal Kelvin wave fronts. The vertical displacement of the isopycnal surfaces associated with these fronts are clearly visible along the north and west coasts on horizontal section of the density fields at the depth of the pycnocline (i.e., 112 m) (Fig. 7b). The resulting dynamical response consists in the generation of a purely baroclinic circulation in geostrophic balance formed of two superimposed gyres, an upper-layer cyclone and a weaker deep anticyclone (Fig. 6b), the vertically averaged associated circulation being zero at least during the first three months. The only significant structure found in the barotropic streamfunction (not shown) is small and weak eddies (~15 km in diameter, 1 to 2 Sv in magnitude) associated with the meanders that develop after three months around the convective area through baroclinic instability process.

### c. *Wind stress and thermohaline forcing (experiment III)*

In experiment III both forcings combine to reinforce the surface cyclonic circulation below the forcing area. In the vicinity of the northern coast, the advection of light surface water by the wind-driven circulation considerably increases the coastal circulation and restricts coastal convection down to 100 m thanks to a continuous supply of relatively warm and fresh water (Fig. 7c) so that the coastal Levantine Intermediate Water is no longer destroyed by the convection (Fig. 8), contrary to what occurs in the absence of wind. The convective region becomes widely detached from the northern coast (~50 km).

The wind-induced barotropic response is not significantly modified by the addition of the thermohaline forcing (Fig. 5) since the thermohaline forcing mainly drives a purely baroclinic circulation (Crépon et al. 1989). The barotropic response appears to be decoupled from the baroclinic one.

After two months the ocean state is thus characteristic of the end of the preconditioning phase of DWF: a broad cyclonic vortex, ~150 km in diameter centered at about 100 km from the northern coast, is formed in the surface layers (first 100 m) with a mean velocity of ~15 cm $s^{-1}$. It overlies a weaker (a few cm $s^{-1}$) and vertically quasi-uniform cyclonic circulation between 500 and 2400 m (Fig. 6c). This vortex surrounds a patch of dense surface water ($\sigma_\theta > 29.00$), 250 m deep more or less at rest (Figs. 6c, 7c). The pycnocline has been removed from the vortex center, leaving very little buoyancy reserve in the water column. The vortex defines the area where further surface cooling and evaporation can lead to deep convection. The local forcing (wind stress plus thermohaline flux) appears to be sufficient to create the preconditioning vortex of DWF.

During the next two months of experiment III, deep convection occurs in the vortex center essentially through the convective adjustment process while the baroclinic adjustment process did play a significant role in previous studies of Madec et al. (1991a) and Madec and Crépon (1991). Indeed, the front surrounding the convective area appears to be baroclinically more stable than in previous experiments. The addition of the surface wind stress tends to impede the meander development that occurred around the convective region in the buoyancy-driven experiment (compare the density fields of Fig. 7b and 7c). Only weak oscillations

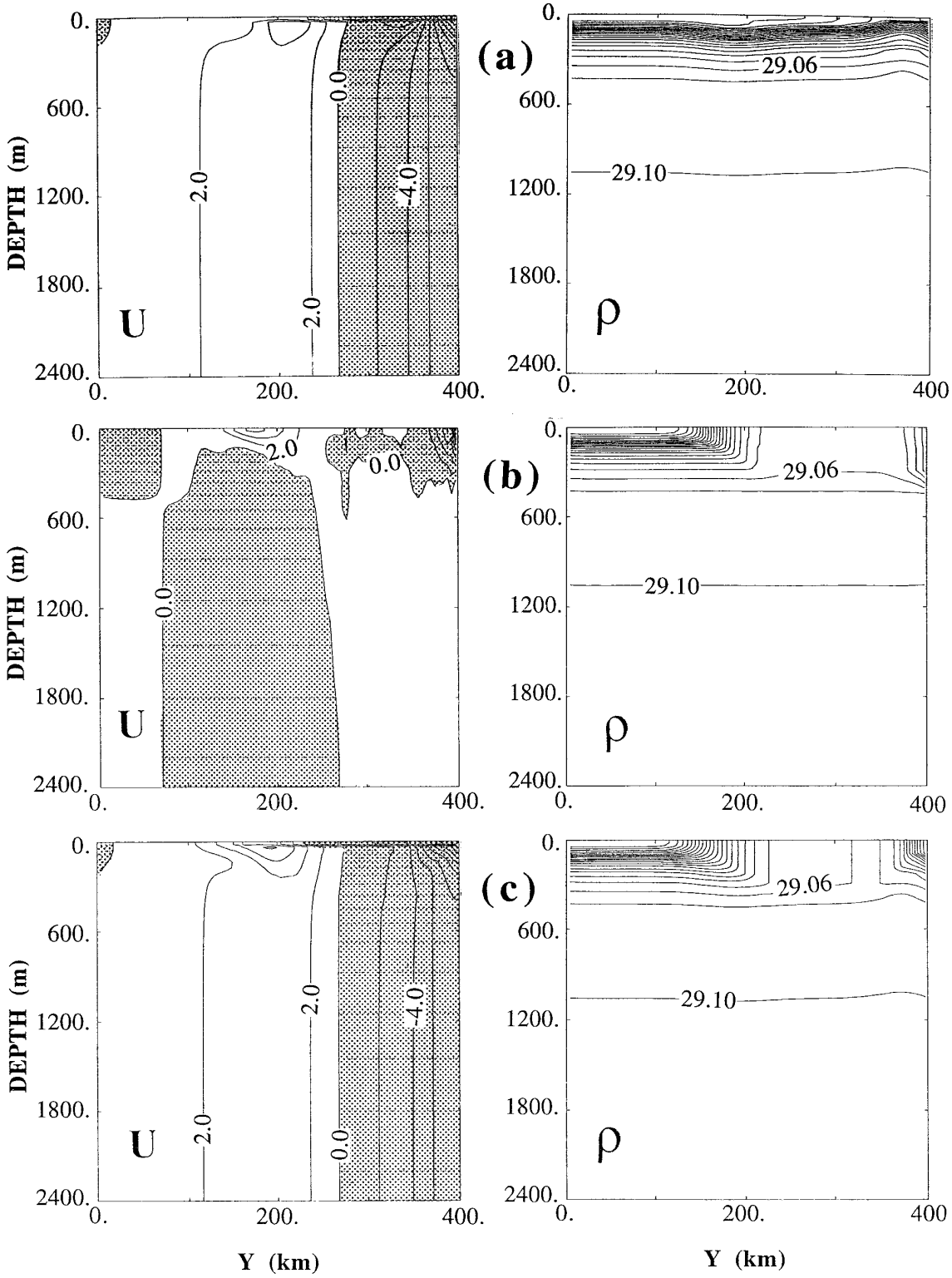


FIG. 6. North–south vertical section of zonal velocity and potential density ($\sigma_\theta$ units) across the convective area ($x$ = 425 km) after 2 months, for (a) experiment I, (b) experiment II, and (c) experiment III. Contour intervals are 2 cm s$^{-1}$ and 0.02 kg m$^{-3}$.

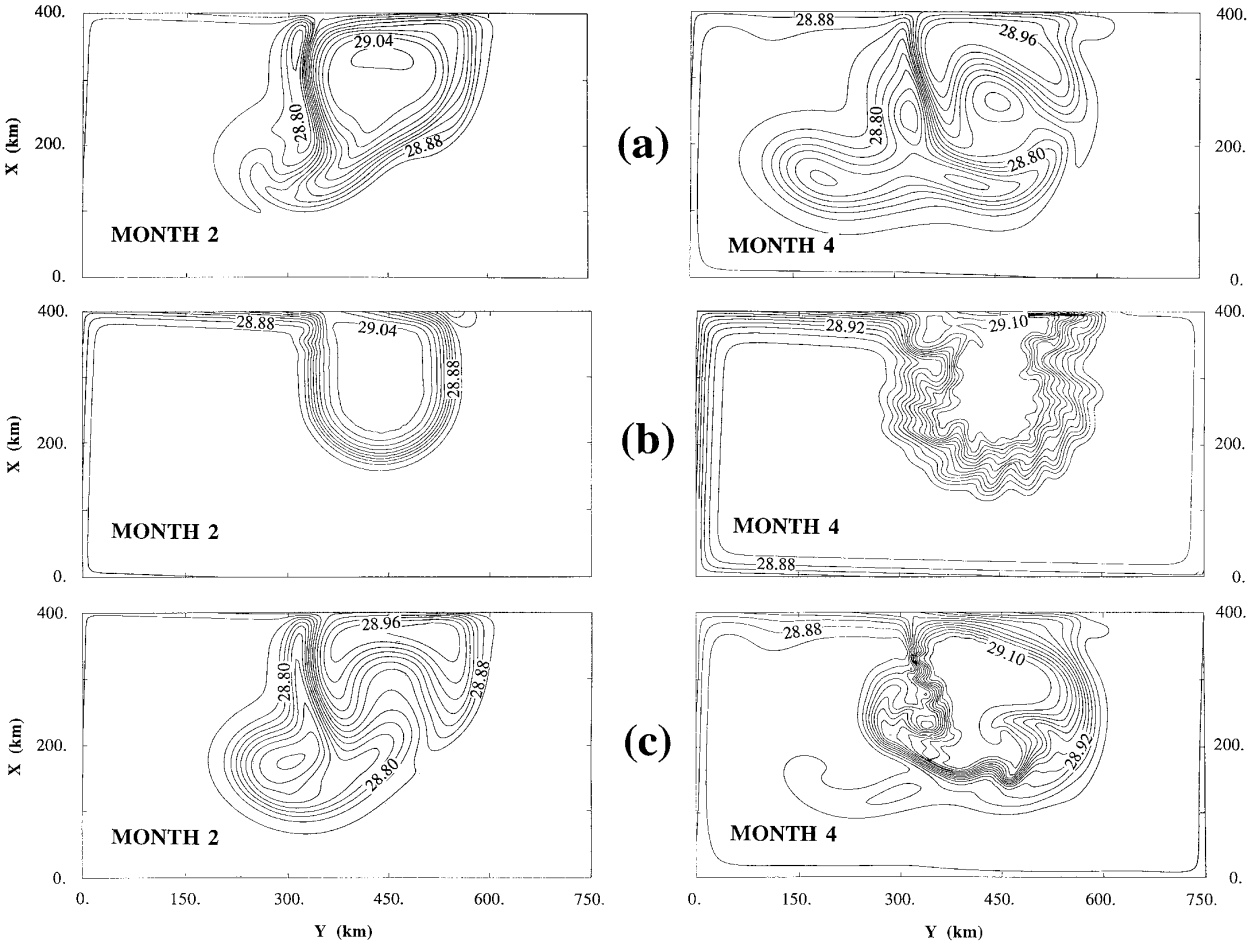


FIG. 7. Horizontal patterns of potential density ($\sigma_\theta$ units) at 112 m after 2 and 4 months for (a) experiment I, (b) experiment II, and (c) experiment III. Contour interval equals 0.02 kg m$^{-3}$.

can be seen on the western side of the vortex during month 3 and 4 (Fig. 7c). The absence of meanders at the periphery of the convective area during the strong cooling period modifies the process driving the convection: the DWF only occurs through the convective process found in nature, which is parameterized by the nonpenetrative convective adjustment algorithm and not through the baroclinic adjustment process linked to the development of baroclinic instabilities (Madec et al. 1991a). A quite significant change is observed in the $T-S$ characteristics of the deep water formed compared to buoyancy-driven experiment II. In experiment III a temperature increase of 0.025°C is found. This weak increase in temperature implies quite a strong heat redistribution since it concerns the whole water column, that is, 2400 m. Assuming a one-dimensional process that mixes the temperature uniformly throughout the water column, a heating of $\sim$24 W m$^{-2}$ would have had to be applied for four months to produce such a temperature increase. This shows that the wind-induced advection in the Ekman layer modifies the water masses involved in the convective process. The horizontal surface dynamics are not negligible anymore in the vortex center.

At the end of the forcing period (month 4), a new water mass is formed which occupies the whole water column in the vortex center (Fig. 8). Its potential temperature and salinity (12.73°C; 38.42‰) are within the range of the observed $T-S$ characteristics of the western Mediterranean deep water reported by Lacombe et al. (1985) and Leaman and Schott (1991). Surface waters present a relative temperature maximum in the vortex center, while a surface temperature minimum is found at the outer edge of the vortex where the convection is not strong enough to extract heat from the heat source linked to the Levantine Intermediate Water. The coastal barotropic advection of peripheral water between the vortex center and the northern coast is sufficient to allow a wide off-coast detachment of the convective area, preventing deep coastal convection (Fig. 8b) so that the Levantine Intermediate Water still persists in the coastal area, in agreement with observations

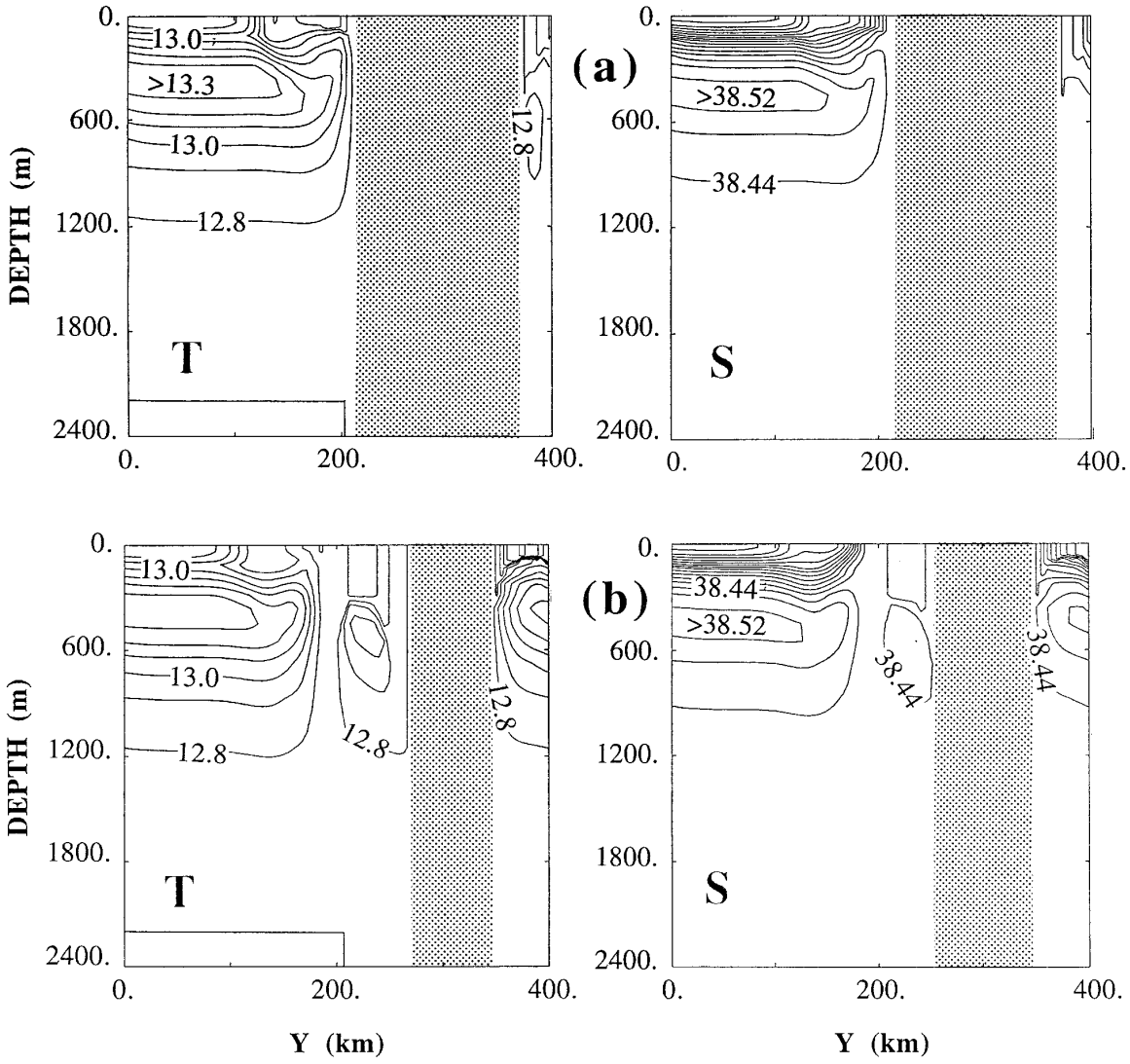


FIG. 8. North–south vertical section of potential temperature and salinity across the convective area ($x$ = 425 km) after 4 months for (a) experiment II and (b) experiment III. Contour intervals are 0.1°C and 0.04 psu, respectively. Dashed areas indicate homogeneous water column from the sea surface to the ocean bottom.

(Tchernia and Fieux 1971). This is not the case in experiment II (Fig. 8a) where the advection of light surface water along the coast only results from the westward coastal current, which is set up after the passage of baroclinic Kelvin wave fronts associated with spatial variation of the thermohaline forcing (Madec and Crépon 1991). Such a advection is not strong enough to prevent a rather deep coastal convection (down to 400 m), which destroys the Levantine Intermediate Water in the coastal area.

## 4. Sensitivity experiments to $\beta$ and topographic effects

The results of the wind-driven experiment have shown that barotropic circulation plays a key role on the preconditioning phase of DWF through advection. DWF occurs in the center of the barotropic cyclone, that is, at the very place where the barotropic advection is negligible. The behavior of the barotropic flow can be explained through the Sverdrup balance between the curl of the wind stress and the $\beta$ effect. To investigate the role of this balance we first present a sensitivity experiment where the $\beta$ effect is suppressed ($\beta = 0$). Furthermore, owing to the strong barotropic component of the circulation generated by the wind stress curl, we expect an effect of the topography on the ocean response. Therefore, a second sensitivity experiment is shown in which a continental shelf and a deep conic bottom topography have been added.

### *a. The f-plane experiment (experiment IV)*

The buoyancy-wind driven experiment (experiment III) has been rerun on a $f$ plane. The barotropic streamfunction and the surface density obtained after 2 and 4 months are displayed in Fig. 9. As in experiment III, the input of positive and negative vorticity due to the wind stress generates a pair of large barotropic gyres of opposite signs but, in the present experiment, the gyres remain nearly symmetrical and continuously strengthen: the ocean response does not evolve toward a steady state since the Sverdrup balance cannot be achieved. The magnitude of the barotropic transport of the gyres reaches 22 Sv after 2 months and more than 30 Sv after 4 months (Fig. 9). The nonlinearities are strong enough to induce a southward propagation of the two gyres by mutual interactions at a speed of a few centimeters per second. The resulting barotropic velocity field is very strong. It presents a southward barotropic jet between the two gyre centers that reaches 20 cm $s^{-1}$ after 4 months. Note that the slight asymmetry observed in Fig. 9 results from the fact that the forcing is not applied in the center of the basin but 125 km east of it.

This drastic change in the barotropic circulation compared to the results of experiment III induces major changes in the thermodynamic structure of the ocean in response to the thermohaline forcing. The southward advection of the whole water column produces a constant renewal of water below the forcing area, while in the south the surface waters cooled by the thermohaline forcing are advected out of the forcing area. There results the formation of a nice mushroomlike surface density structure as dense surface waters are advected around each gyre (Fig. 9). Surface waters are not trapped below the forcing area anymore but continuously replaced by light peripheral waters coming symmetrically from the west and east sides of the forcing area. This yields a strong decrease of the surface density compared to experiment III. Its maximum value is found after 4 months when it is less than 29.00, much too light to generate deep convection and form deep water (Fig. 9). In experiment IV the depth of convection never exceeds 200 m. This sensitivity experiment confirms the paramount role played by the barotropic circulation in the DWF process, and consequently the key role of $\beta$ effect, which strongly influences this circulation.

### *b. Effect of bottom topography*

As was early emphasized by Swallow and Gaston (1973) and Hogg (1973), the bottom topography can be of importance in DWF. We now investigate the possible influence of the Deep Sea Fan of the Rhône River and coastal geometry on the DWF by running a fifth

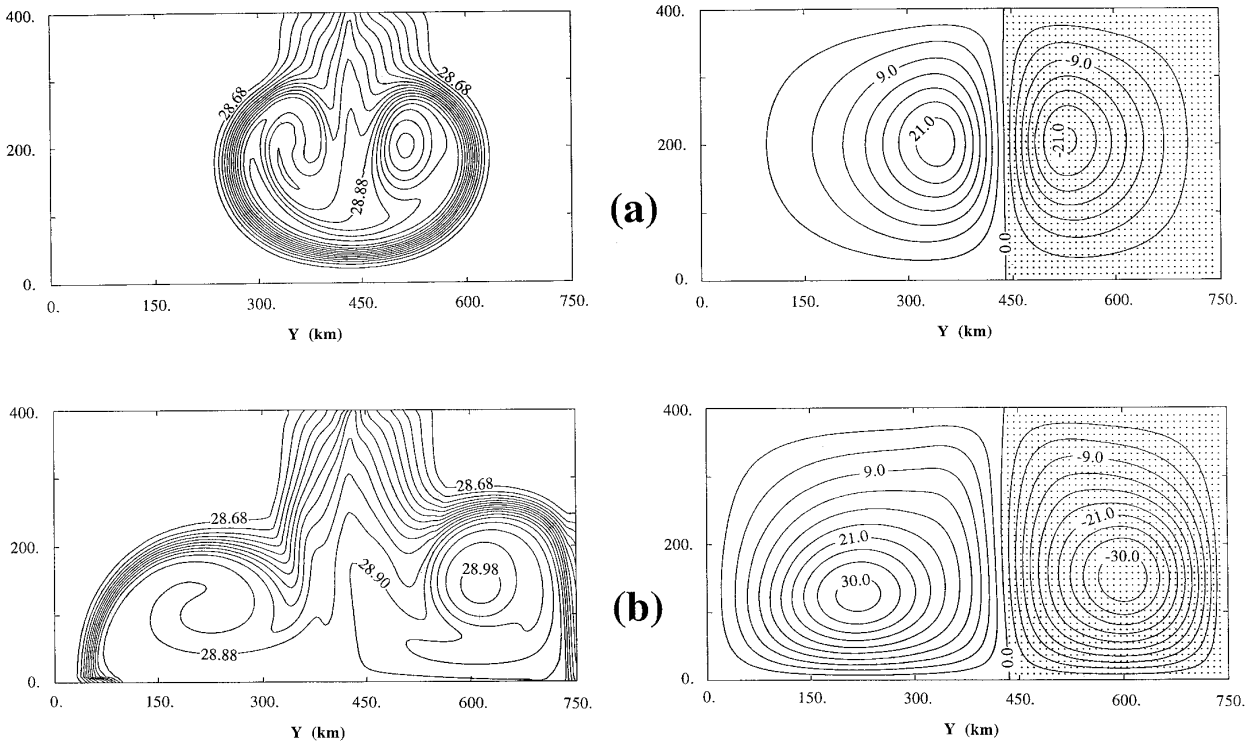


FIG. 9. Horizontal patterns of surface density ($\sigma_\theta$ units) and barotropic streamfunction after (a) 2 and (b) 4 months for experiment IV. Contour intervals equal 0.02 kg $m^{-3}$ and 3 Sv.

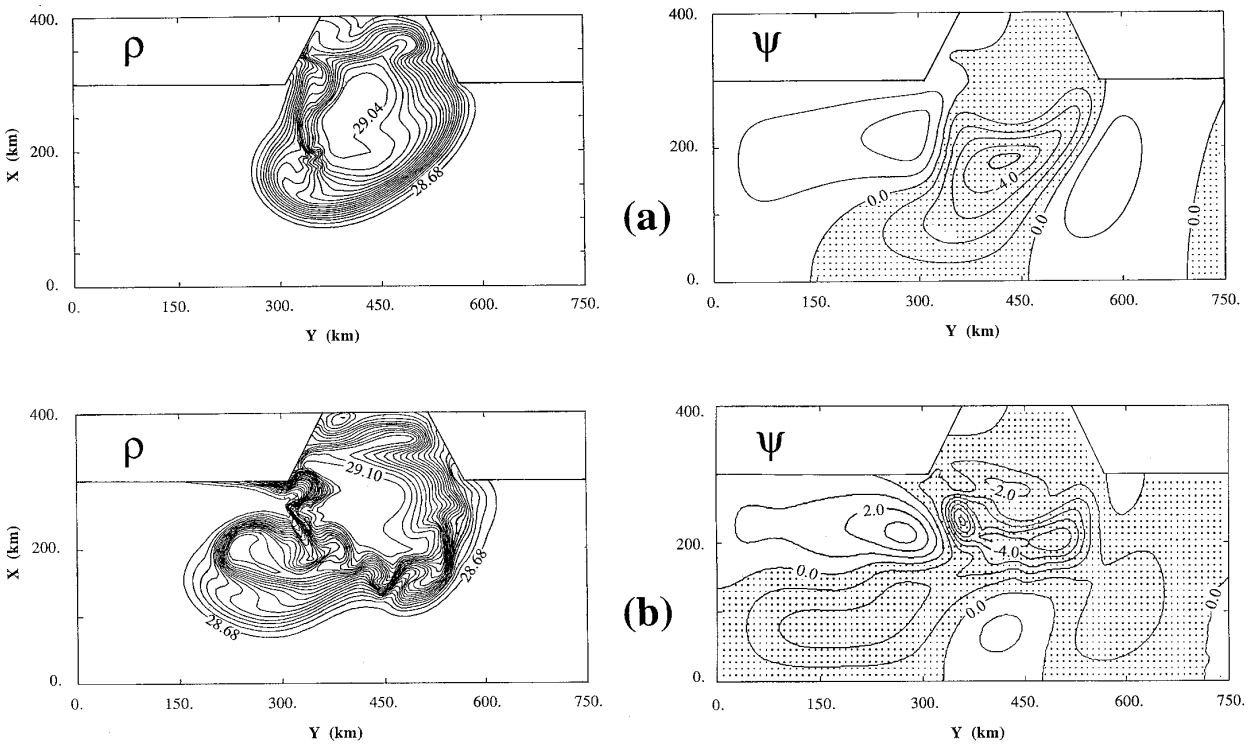


FIG. 10. Horizontal patterns of surface density ($\sigma_\theta$ units) and barotropic streamfunction after (a) 2 and (b) 4 months for experiment V. Contour intervals equal 0.02 kg m$^{-3}$ and 1 Sv.

experiment (experiment V) similar to experiment III but where a continental shelf and a deep conic bottom topography have been added.

Let us define $H$ as the depth of the ocean, $H_0$ and $L$ as the vertical and horizontal scale of the bottom topography. At small Rossby number $U/fL$ it is found that a barotropic geostrophic flow moves along the isobaths of the bottom topography if the aspect ratio $H_0/H$ is $O(1)$ (Pedlosky 1979, p. 89). In experiment V, a typical barotropic velocity $U$ is 5 cm s$^{-1}$ and the length scale of the topography is $L_1 = 40$ km for the continental slope of the Golfe du Lion and $L_2 = 100$ km for the Rhône Deep Sea Fan. In both cases the Rossby number is of the order of $10^{-2}$. With the topography defined in section 2, the aspect ratios are of the order of 0.5 so that the dynamical influence of the topography is expected to predominate, that is, the flow would tend to move along the isobaths of the bottom topography according to the arguments developed in Pedlosky (1979).

The barotropic ocean response obtained in experiment V is in good agreement with the above analysis. The positive and negative input of vorticity induced by the wind first generates an anticyclonic and a cyclonic barotropic gyre, respectively, located on each side of the forcing area. Their meridional extension and their magnitude are smaller than in experiment III since the northern coast has been shifted 100 km southward, reducing the forcing area over the deep ocean. By radiating topographic Rossby waves, the response evolves toward a single cyclonic barotropic gyre located below the forcing area (Fig. 10). The shape of this barotropic cyclone is not only constrained by the applied wind stress field as in experiment I and III but also by the bottom topography. Due to the large value of the aspect ratio the flow tends to follow the bathymetric contours and remains confined in the deep ocean region, that is, enters neither over the Rhône Deep Sea Fan nor over the continental shelf. Therefore, the center of the barotropic cyclone generated by the wind stress is shifted southward due to the topography (Fig. 10a). The transport of the barotropic cyclone is equal to ~5 Sv, which is about three times smaller than in the case with a flat bottom (experiment III). This transport reduction is due to the reduction of the forcing area and to the fact that the topography $\beta$ effect is much larger than the planetary $\beta$ effect that yields a smaller transport when the Sverdrup balance is applied. The barotropic velocity along the cone is 5 cm s$^{-1}$ (Fig. 11), which is somewhat smaller than the velocity found along the coast in experiment III. Nevertheless, this barotropic velocity is strong enough to interact with the bottom topography and becomes an essential ingredient of the preconditioning phase.

The surface density fields at months 2 and 4 are displayed in Fig. 10b. As the atmospheric fluxes can act

a longer time on water masses remaining at the same location convection occurs at the place where the ocean advection is minimum and the atmospheric fluxes maximum. Since the barotropic flow follows the bathymetric contour of the fan, a water column remains trapped over it during the whole simulation. Therefore, a patch of dense water forms over the fan and below the forcing area. As in experiment III, this low advection area becomes the place where the buoyancy forcing is the most efficient to generate strong vertical mixing. This zone becomes a privileged zone for deep convection to occur thereafter. But in opposition to experiment III, the dense surface water zone is no longer located in the center of the barotropic cyclone, which is displaced southward but is north of it, over the fan. The southward extension of the patch of dense surface water is limited by the barotropic advection of light water around the fan.

During the next two months, the convection reaches deeper layers over the fan while the surface density increases, exceeding 29.10 at month 4 over a large area (Fig. 10b). At the end of this period the convection occurs down to the bottom over an oval area 100 km $\times$ 50 km extending from the center of the fan to its western side (Figs. 10 and 11).

The dynamic constraint of the Rhône Fan appears to be of fundamental importance in triggering DWF. The area where DWF occurs is located over the fan (i.e., abutted to the continental slope), in agreement with the observations (Swallow and Gaston 1973). This was also Hogg's (1973) conclusion, but the mechanism invoked here is quite different. Hogg invoked the role played by the sign and magnitude of the lateral shear of the fluid (parameter $\gamma$) and the vertical shear normalized by the aspect ratio (parameter $\beta$) in generating a ''Taylor column'' trapping the surface waters. For certain regions of the ($\gamma$, $\beta$) space a ''Taylor column'' appears. In the present study, the arguments invoked are much simpler and are linked to the conservation of potential vorticity, which constrains the flow to move along the isobaths of the bottom topography.

Additional sensitivity experiments (not shown) performed without the continental shelf simulating the Gulf of Lion have shown that DWF occurring over the fan is not so efficient as in presence of a continental shelf. The main reason is that the surface waters do not exactly follow the deep water motions. The latter have a tendency to follow the isobaths of the bump unlike the former, which remain trapped along the coast. When there is no continental shelf this leads to a continuous water replacement over the fan. This advection limits the DWF in the Fan area, so that deep convection never reach the ocean bottom. On the contrary, when the continental shelf is present, the surface current penetrates the shelf following the shelf isobaths and leaving the Fan area quiescent. Both topographic features (the continental shelf and the fan) participate to the selection of the area where DWF occurs.

## 5. Discussion and conclusions

The large-scale processes preconditioning the DWF in the Western Mediterranean have been investigated by performing several numerical experiments. We used the three-dimensional primitive equation model developed at the LODYC. Convection was parameterized by a simple nonpenetrative convective adjustment algorithm suitable to reproduce the major mesoscale and large-scale features associated with DWF (Madec et al. 1991a,b; Send and Marshall 1993). Attention was focused on the ocean response to the local atmospheric forcing (thermohaline fluxes and wind stress) having the gross features of mean winter forcing found in the MEDOC area and then on the effect bottom topography. The major conclusions are as follows:

The curl of the wind stress is responsible for a baroclinic motion and a barotropic motion. The baroclinic motion is induced by Ekman pumping. It is associated with small vertical displacements of isopycnal surfaces of about 50 m, which do not significantly influence DWF. After a spinup phase corresponding to the time for the barotropic planetary Rossby waves to be radiated away, the barotropic flow forms a large (diameter of about 100 km) and strong (18 Sv) barotropic cyclone trapped under the forcing area. The barotropic motion fits the Sverdrup balance between the planetary vorticity and the wind stress curl. The computed transport is only 5% (1 Sv) higher than the one obtained from the Sverdrup balance. This barotropic circulation has a major effect on the preconditioning phase of DWF and thus on the DWF itself. Indeed, adding a thermohaline forcing to the wind stress field causes the formation of a patch of dense water in the center of the barotropic cyclone. This dense water patch, which is linked to the barotropic cyclone, is widely detached from the northern coast and defines the area where DWF occurs during the winter period. Therefore, the wind stress curl is responsible for an efficient preconditioning. A barotropic water column is trapped in the cyclone center so that it is exposed to evaporation and cooling throughout the winter. With the thermohaline forcing considered here, this effect is sufficient to drive deep convection in the vortex center (Madec et al. 1991a). At its periphery, the water column is advected at a speed of a few centimeters per second, which strongly reduces its buoyancy loss since the forcing is localized in a narrow strip. Taking a current of 5 cm $s^{-1}$, which is the typical value both measured in this area (Schott and Leaman 1991) and found in Experiment V, a water column crosses the forcing area (200 km) in only 40 days. The water feels the atmospheric forcing for quite a short time, the thermohaline budget is reduced and not enough buoyancy can be extracted to drive deep convection. As a consequence the westward barotropic advection induces a detachment of $\sim$100 km of the convective area off the north-

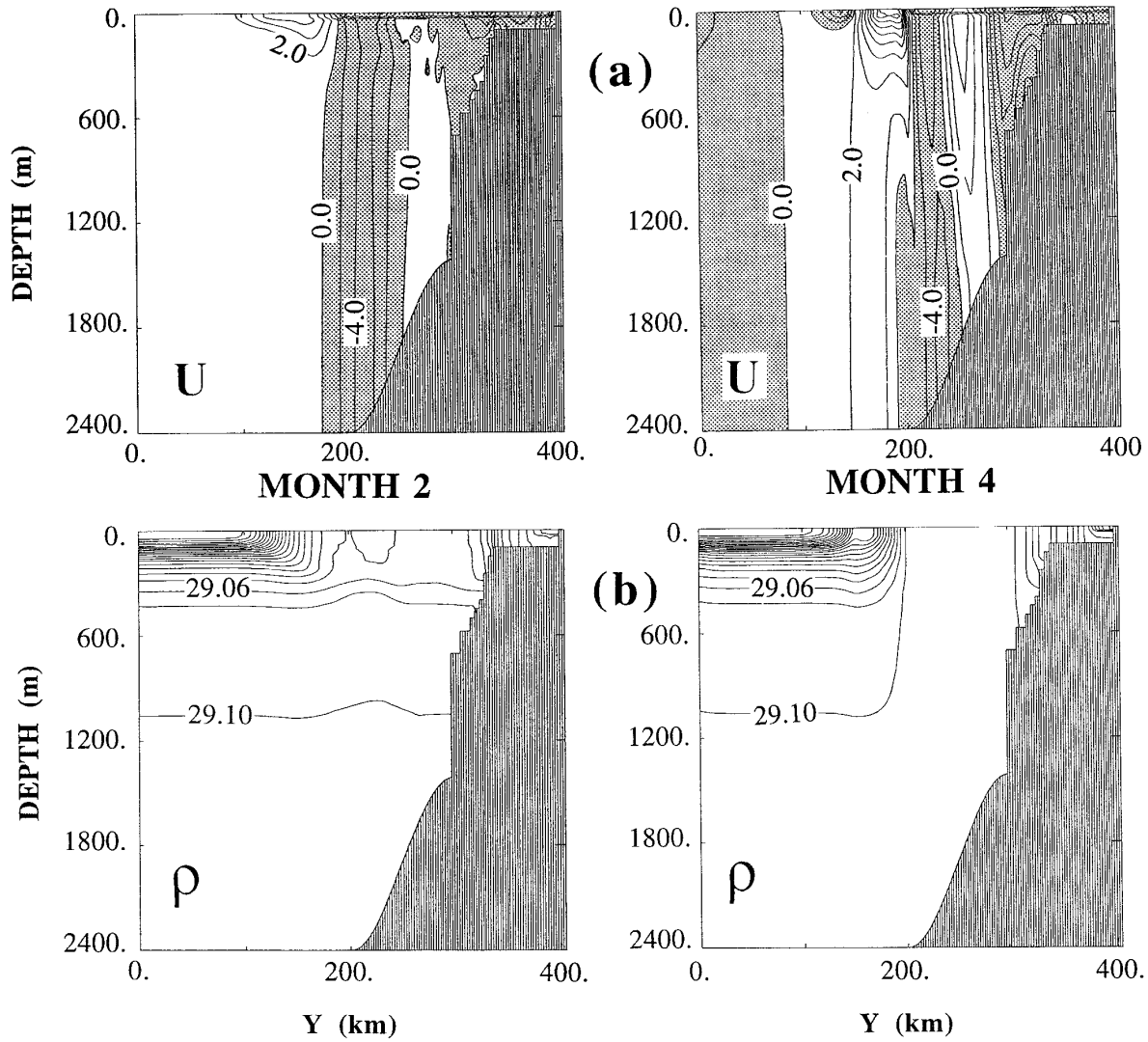


FIG. 11. North–south vertical section of (a) zonal velocity, (b) potential density ($\sigma_\theta$ units), (c) temperature, and (d) salinity across the convective area ($x$ = 425 km) after 2 and 4 months for experiment V. Contour intervals are 2 cm s$^{-1}$, 0.02 kg m$^{-3}$, 0.1°C, and 0.04 psu. Dashed areas in (c) and (d) indicate homogeneous water column from the sea surface to the ocean bottom.

ern coast, a length scale that corresponds to the width of the barotropic current.

In addition to its effect on the *preconditioning* phase of DWF, the wind stress acts on the *violent* mixing phase. It tends to inhibit the meander development at the vortex periphery, which was occurring in the buoyancy-driven experiment. For that reason, it modifies the DWF process, promoting the *convective* process to the detriment of the *baroclinic adjustment* process. Moreover the wind-induced advection within the Ekman layer changes the water masses involved in the convection, leading to significantly different $T$–$S$ characteristics of the deep water.

To emphasize the key role played by the barotropic circulation on the preconditioning phase of DWF in the northwestern Mediterranean Sea, two additional sensitivity experiments have been performed, checking the importance of the $\beta$ effect and the bottom topography. Running the buoyancy-wind driven experiment on a $f$ plane induces a drastic change in the barotropic flow since the Sverdrup balance is no longer possible. The barotropic flow becomes a strong southward jet located at the place where the wind is maximum. Mass continuity is ensured by two symmetrical water cells situated on the east and west sides of the forcing area. This generates a permanent renewal of the water column below the forcing area and drastically reduces the depth of convection to a maximum of 200 m after 4 months of simulation. Adding a Rhône Deep Sea Fan also strongly affects the barotropic response to the wind

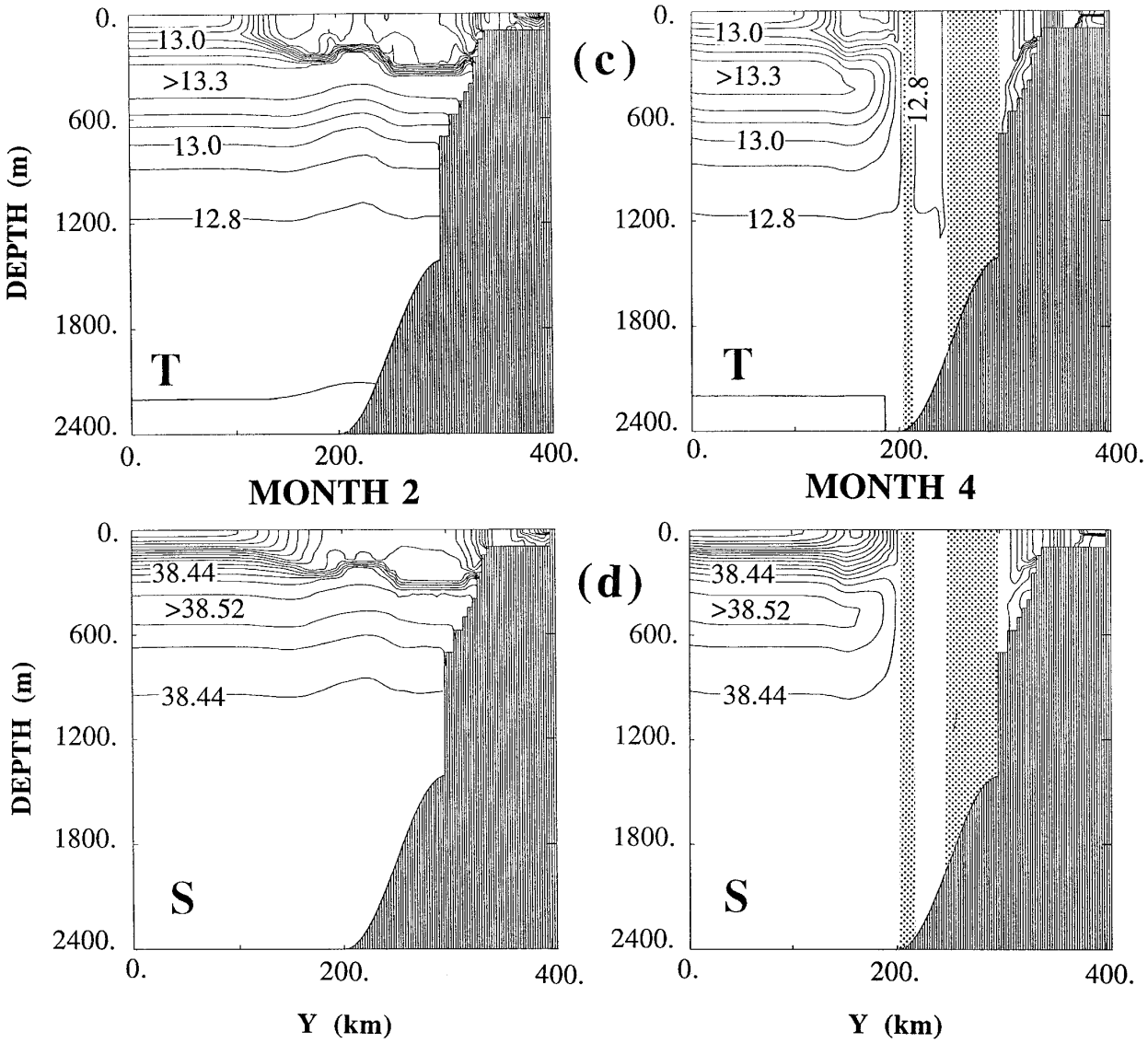


FIG. 11. (*Continued*)

stress and thus DWF. The barotropic flow is constrained to follow the bathymetry contours. The fluid above the fan remains quiescent all along the simulation and thermohaline fluxes can act a long enough time on the same water mass to trigger DWF. Therefore, a patch of dense water forms above the Rhône Fan. It is limited to the north by the advection of light surface water, which enters the continental shelf, and to the south by the westward barotropic advection, which follows the bathymetric contours. This patch defines the area where DWF occurs at the end of the winter period. The invoked mechanism is related to fluid advection rather than to the formation of a Taylor column as suggested by Hogg (1973).

If strong negative buoyancy flux is a necessary condition for DWF, it is not a sufficient one, especially in the MEDOC area where the strong air–sea interactions are localized due to the channeling of the wind by the mountains. Indeed, DWF only happens if water masses are exposed to strong buoyancy forcing during a sufficient time. When the forcing is localized, ocean advection controls the time of exposure to the forcing and thus the DWF. In this study, the wind, through the barotropic advection it drives, has been found to exert such a control. Nevertheless, the wind stress used is obviously a simplified representation of the actual one, which has a strong time and space variability in the MEDOC area. Whatever the influence of such a vari-

ability on the flat bottom response, the presence of the Rhône Deep Sea Fan exerts a powerful and permanent control on the barotropic circulation, preventing strong barotropic advection above the fan itself. The Rhône Deep Sea Fan is thus a major ingredient of the DWF in the northwestern Mediterranean Sea.

*Acknowledgments.* This work is a contribution of MAST 1 EUROMODEL and MEDMODEL Programs. Funding has been provided by the CEE under the MAST program (MAST 93.C) and by the following French governmental agencies: Direction des Recherches et Etudes Techniques (DRET 90.376), Centre National de la Recherche Scientifique (CNRS), and Ministère de l'Environnement. Support for computation has been provided by the Institut de Recherche en Informatique Scientifique (IDRIS) du CNRS.

## REFERENCES

Anati, D. A., 1971: On the mechanism of the deep mixed layer formation during MEDOC 69. *Cah. Oceanogr.,* **23**(4), 427–443.

——, and H. Stommel, 1970: The initial phase of deep water formation in the Northwest Mediterranean, during MEDOC 69, on the basis of observations made by ''ATLANTIS II'', January 25–February 12, 1969. *Cah. Oceanogr.,* **22**(4), 343–351.

Andrich, P., P. Delecluse, C. Levy, and G. Madec, 1988: A multitasked general circulation model of the ocean. *Science and Engineering on Cray Supercomputers, Proc. of the Fourth Int. Symp.,* Minneapolis, MN, A Cray Research book, 407–428.

Bunker, A. F., 1972: Wintertime interactions of the atmosphere with the Mediterranean Sea. *J. Phys. Oceanogr.,* **2,** 225–238.

Crépon, M., L. Wald, and J. M. Monget, 1982: Low-frequency waves in the Ligurian Sea during December 1977. *J. Geophys. Res.,* **87**(C1), 595–600.

——, M. Boukthir, B. Barnier, and F. Aikman III, 1989: Horizontal ocean circulation forced by deep-water formation. Part I: An analytical study. *J. Phys. Oceanogr.,* **19,** 1781–1792.

Delecluse, P., G. Madec, M. Imbard, and C. Lévy, 1993: OPA Version 7 Ocean General Circulation Model reference manual. LODYC, France, Internal Rep. 93/05, 111 pp.

Eckart, C., 1958: Properties of water. Part II: The equation of state of water and sea water at low temperatures and pressures. *Amer. J. Sci.,* **256,** 225–240.

Fieux, M., 1972: Contribution à l'étude hydrologique et dynamique du Golfe du Lion en période hivernale. Thèse de la Faculté des Sciences de Paris, 90 pp.

Gascard, J. C., 1978: Mediterranean deep water formation, baroclinic instability and oceanic eddies. *Oceanol. Acta,* **1**(3), 315–330.

Gary, J. M., 1973: Estimate of truncation error in transformed coordinate primitive equation atmospheric models. *J. Atmos. Sci.,* **30,** 223–233.

Gerdes, R., 1993: A primitive equation ocean circulation model using a general vertical coordinate transformation. Part I: Description and testing of the model. *J. Geophys. Res.,* **98,** 14 683–14 701.

Hogg, N. G., 1973: The preconditioning phase of MEDOC 1969-II. Topographic effects. *Deep-Sea Res.,* **20,** 449–459.

Jones, H., and J. Marshall, 1993: Convection with rotation in a neutral ocean: A study of open-ocean deep convection. *J. Phys. Oceanogr.,* **23,** 1009–1039.

Killworth, P. D., 1976: The mixing and spreading phases of MEDOC. I. *Progress in Oceanography,* Vol. 7, Pergamon, 59–90.

——, 1989: On the parameterization of deep convection in ocean models. *Parameterization of Small-Scale Processes. Proc. Hawaiian Winter Workshop,* University of Hawaii at Manoa, 59–74.

Lacombe, H., P. Tchernia, and L. Gamberoni, 1985: Variable bottom water in the western mediterranean basin. *Progress in Oceanography,* Vol. 14, Pergamon, 319–338.

Leaman, K. D., and F. Schott, 1991: Hydrographic structure of the convection regime in the Gulf of Lions: Winter 1987. *J. Phys. Oceanogr.,* **21,** 575–598.

Lott, F., G. Madec, and J. Verron, 1990: Topographic experiments in an Ocean General Circulation Model. *Ocean Modelling* (unpublished manuscript), **88,** 5–7.

Madec, G., and M. Crépon, 1991: Thermohaline driven deep water formation in the north-western Mediterranean sea. *Deep Convection and Deep Water Formation in the Oceans,* P. C. Chu and J.-C. Gascard, Eds., *Elsevier Oceanogr. Ser.,* 241–265.

——, M. Chartier, P. Delecluse, and M. Crépon, 1991a: A three-dimensional numerical study of deep-water formation in the northwestern Mediterranean Sea. *J. Phys. Oceanogr.,* **21,** 1349–1371.

——, ——, and M. Crépon, 1991b: Effect of thermohaline forcing variability on deep-water formation in the western Mediterranean Sea: A high resolution 3D numerical study. *Dyn. Atmos. Oceans,* **15,** 301–332.

Marti, O., G. Madec, and P. Delecluse, 1992: Comment on ''Net diffusivity in ocean general circulation models with nonuniform grids.'' *J. Geophys. Res.,* **97**(C8), 12 763–12 766.

May, P. W., 1982: Climatological flux in Mediterranean Sea. Part I: Winds and wind stresses. Naval Ocean Research and Development Activity, NSTL station, MS. NORDA Tech. Rep. 54, 56 pp.

McCreary, J. P., H. S. Lee, and D. B. Enfield, 1989: The response of the coastal ocean to strong offshore winds: With application to circulations in the Gulfs of Tehuantepec and Papagayo. *J. Mar. Res.,* **47,** 81–109.

MEDOC Group, 1970: Observation of formation of deep water in the Mediterranean Sea, 1969. *Nature,* **227,** 1037–1040.

Meteorological Office, 1962: *Weather in the Mediterranean.* M.O. 391, Vol. 1.

Pacanowski, R. C., and S. G. H. Philander, 1981: Parameterization of vertical mixing in numerical models of tropical oceans. *J. Phys. Oceanogr.,* **11,** 1443–1451.

Pedlosky, J., 1979: *Geophysical Fluid Dynamics.* Springer-Verlag, 624 pp.

Schott, F., and K. D. Leaman, 1991: Observations with moored acoustic Doppler current profilers in the convection regime in the Golfe du Lion. *J. Phys. Oceanogr.,* **21,** 558–574.

——, K. M. Visbeck, and U. Send, 1993: Open ocean deep convection, Mediterranean and Greenland Seas. *Ocean Processes in Climate Dynamics: Global and Mediterranean Examples,* P. Malanotte-Rizzoli and A. R. Robinson, Eds., Kluwer Academic, 203–225.

Send, U., and J. Marshall, 1995: Integral effects of deep convection. *J. Phys. Oceanogr.,* **25,** 855–872.

Swallow, J. C., and G. F. Caston, 1973: The preconditioning phase of MEDOC 1969—I. *Deep-Sea Res.,* **20,** 429–448.

Tchernia, P., and M. Fieux, 1971: Résultats des observations hydrologiques exécutées à bord du N/O ''Jean Charcot'' pendant la campagne MEDOC 69 (30 janvier–28 février), (18–31 mars). *Cah. Océanogr.,* **23**(Suppl. 1), 1–91.